blood®
Regular Article

HEMATOPOIESIS AND STEM CELLS

Cytokine combinations for human blood stem cell expansion induce cell-type– and cytokine-specific signaling dynamics

Weijia Wang,[1,*] Yang Zhang,[1*] Philip Dettinger,[1] Andreas Reimann,[1] Tobias Kull,[1] Dirk Loeffler,[1] Markus G. Manz,[2] Claudia Lengerke,[3,4] and Timm Schroeder[1]

[1]Department of Biosystems Science and Engineering, Eidgenössische Technische Hochschule (ETH) Zurich, Basel, Switzerland; [2]Department of Medical Oncology and Hematology, University Hospital Zurich–University of Zurich, Comprehensive Cancer Center Zurich, Zurich, Switzerland; [3]Department of Biomedicine, University Hospital Basel–University of Basel, Basel, Switzerland; and [4]Department of Internal Medicine, Hematology, Oncology, Clinical Immunology and Rheumatology, University Hospital Tübingen, Tübingen, Germany

KEY POINTS

- Combined biosensors, time-lapse imaging, and microfluidics enable signaling dynamics quantification in live HSPCs.
- Human HSPC ERK signaling dynamics are heterogeneous and specific for cytokines and their combinations in a cell-type–dependent manner.

How hematopoietic stem cells (HSCs) integrate signals from their environment to make fate decisions remains incompletely understood. Current knowledge is based on either averages of heterogeneous populations or snapshot analyses, both missing important information about the dynamics of intracellular signaling activity. By combining fluorescent biosensors with time-lapse imaging and microfluidics, we measured the activity of the extracellular-signal–regulated kinase (ERK) pathway over time (ie, dynamics) in live single human umbilical cord blood HSCs and multipotent progenitor cells (MPPs). In single cells, ERK signaling dynamics were highly heterogeneous and depended on the cytokines, their combinations, and cell types. ERK signaling was activated by stem cell factor (SCF) and FMS-like tyrosine kinase 3 ligand in HSCs but SCF, interleukin 3, and granulocyte colony-stimulating factor in MPPs. Different cytokines and their combinations led to distinct ERK signaling dynamics frequencies, and ERK dynamics in HSCs were more transient than those in MPPs. A combination of 5 cytokines recently shown to maintain HSCs in long-term culture, had a more-than-additive effect in eliciting sustained ERK dynamics in HSCs. ERK signaling dynamics also predicted future cell fates. For example, CD45RA expression increased more in HSC daughters with intermediate than with transient or sustained ERK signaling. We demonstrate heterogeneous cytokine- and cell-type–specific ERK signaling dynamics, illustrating their relevance in regulating hematopoietic stem and progenitor (HSPC) cell fates.

Introduction

Hematopoietic stem and progenitor cells (HSPCs) are controlled by cell-extrinsic signals like cytokines to meet the changing demand for blood cell production.[1-7] Alterations in signaling processes also drive leukemic transformation.[8-11] Therefore, understanding the underlying mechanisms is important for developing strategies to direct normal or leukemic HSPC responses in vivo and in vitro. However, how HSPCs integrate external signals through intracellular signaling networks to determine cell fate (eg, self-renewal vs differentiation, survival, proliferation, and lineage choice) remains largely undefined. Optimal signaling inputs for expansion of human hematopoietic stem cells (HSCs) are not understood, and current culture conditions are limited in supporting the expansion of these cells.[12] The in vivo HSC signaling environment is complex and dynamic, consisting of many factors with distinct temporal and dose patterns.[13-15] These can lead to unpredictable nonlinear signaling responses,[16,17] in part due to the complex and highly interconnected intracellular "signal processing" network.

Cytokines engage specific intracellular signaling pathways, rapidly eliciting responses depending on, for example, cytokine concentration, combinations and temporal patterns, and the type or current state of the receiving cell.[7,18,19] Individual stimuli typically activate multiple signaling pathways, and the resulting cytokine-specific combinations may thus induce specific cell fates. However, despite leading to different cell fate choices, different stimuli often activate overlapping pathways.[7,18,20] In addition, signaling activity over time (ie, dynamics), rather than just on/off activation state, can be specific for the receiving cell type, as well as for the type, concentration, or temporal pattern of stimulation.[18,21-24] This extends the parameter space in which cells can compute their reaction to stimuli. It has recently become clear that these dynamics (eg, sustained, transient, or oscillatory) dictate cellular fate outcomes.[23] In PC-12 cells, transient vs sustained activity of

extracellular signal–regulated kinase (ERK) leads to proliferation and differentiation, respectively.[24] Here, manipulation of ERK activation patterns by temporally controlled cytokine stimulation has provided direct evidence that ERK signaling dynamics controls PC-12 cell fate decisions.[22]

Recent advancement in fluorescent signaling biosensors[25] and time-lapse imaging[26-28] enable the continuous quantification of signaling activity in live single cells. For example, kinase translocation reporters (KTRs) are fluorescent biosensors which are phosphorylated by specific kinases, leading to their export from the nucleus. This shift of fluorescence from the nucleus to the cytoplasm thus allows the quantification of kinase activation over time.[29,30] Quantification of signaling activity dynamics revealed that population-level signaling activity measurements are not reflective of how individual cells respond.[31-33] Even in isogenic cells of the PC-12 cell line, stimulation with the same cytokine leads to heterogeneity in ERK signaling dynamics and subsequent cellular outcomes at the single-cell level.[22,34] Quantifying signaling activity dynamics is therefore important to understand cell fate control. However, previous studies were mostly done in easy to culture and manipulate cell types or lines. Analyses of difficult-to-obtain, culture, and manipulate primary HSPCs have been lacking, mostly because of lacking technologies. Due to context-dependent interconnectivity between signaling nodes,[35,36] the nonlinearity in signaling response to multiple inputs,[16,17] and the functional heterogeneity displayed by human HSPCs in vitro and in vivo,[37,38] it is crucial to measure signaling dynamics in individual human HSPCs over time upon delivery of combined cytokines with known concentration and stimulation dynamics.[18,27,39-41]

Quantification of signaling dynamics in human HSPCs therefore requires their culture in defined media, rapid change of media without cell displacement, and sensitive microscopy for cell tracking and fluorescence quantification. In addition, efficient cell capture during loading into the culture device is crucial for precious HSPCs, which are available only in very low numbers. Therefore, we developed a novel microfluidic cell culture platform that enables efficient capture and culture of HSPCs, rapid stimulation of these suspension cells without cell displacement through diffusion, automated temporally controlled delivery of chemically defined media, and continuous observation of cells by time-lapse imaging with optimized sensitivity.[42]

Here, we combined an ERKKTR biosensor[29] with time-lapse imaging and microfluidics to quantify ERK signaling dynamics in live single human umbilical cord blood (UCB)-derived HSCs and MPPs. For stimulation, we used individual and combinations of cytokines contained in recently reported culture conditions supporting HSC maintenance or expansion in culture.[43-45] ERK signaling dynamics were heterogeneous at the single-cell level, and different cytokines and their combinations led to specific distributions of distinct ERK signaling dynamics in a cell-type–specific manner.

Methods

Ethical statement

Anonymized human UCB samples were collected from healthy newborns of both sexes at the University Hospitals Basel or Zurich (Department of Obstetrics, University Hospital Zurich and Triemli Hospital, Zurich, Switzerland) with parental informed consent. Relevant ethical regulations were followed, according to the guidelines of the local Basel ethics committees (vote 13/2007V, S-112/2010, EKNZ2015/335) or the ethics boards of the canton Zurich (KEK-StV-Nr. 40/14).

HSC and MPP cell isolation

UCB cells were processed by density gradient centrifugation, and $CD34^+$ cells were isolated using EasySep CD34 Positive Selection Kit II (samples from Basel, catalog no. 17896; Stemcell Technologies) or positive immunomagnetic selection with anti-human CD34 microbeads (samples from Zurich, Miltenyi Biotec) and frozen. Before fluorescence-activated cell sorting (FACS), they were thawed, resuspended in prewarmed FACS buffer (phosphate-buffered saline; 2% fetal calf serum), and stained with antibodies against CD34-allophycocyanin (APC) (clone 581; BD Biosciences), CD38-phycoerythrin (PE)-Cy7 (HB7; BioLegend), CD90-PE (5E10; BD Biosciences), CD45RA-fluorescein isothiocyanate (HI100; BioLegend), and CD49f-PE-Cy5 (GoH3; BD Biosciences) for 30 minutes on ice. Cells were then washed and resuspended in FACS buffer with 1 μg/mL aminoactinomycin (7-AAD). HSC ($CD34^+CD38^-CD45RA^-CD90^+CD49f^+$) and MPP ($CD34^+CD38^-CD45RA^-CD90^-CD49f^-$) populations were sorted using a BD FACSAria III with a 100-μm nozzle, purity mode, and sorting purities ≥90%. Gates and thresholds were set according to fluorescence minus 1 control as depicted in supplemental Figure 1 (available on the *Blood* Web site)

Lentivirus production and transduction

ERKKTR (#59138; Addgene)[29] was fused to the fluorescent protein monomeric RUBY2 (mRUBY2),[46] linked with VENUS[47] nucmem[48] by the picornavirus 2A sequence, and cloned into vesicular stomatitis virus G pseudotyped lentivirus[26] (third generation) constructs using the In-Fusion Cloning System (Takara Bio). Virus was produced and titrated as previously described.[26] HSCs and MPPs were prestimulated overnight (12-16 hours) and then subjected to 48 hours of transduction in a serum-free medium containing phenol red–free Iscove modified Dulbecco medium (catalog no. 21056-023; GIBCO) supplemented with 20% BIT (catalog no. 09500; Stemcell Technologies), 1% Glutamax (catalog no. 35050-038; GIBCO), 1% penicillin-streptomycin (catalog no. 15140-122; GIBCO), 40 μg/mL low-density lipoproteins (catalog no. 02698; Stemcell Technologies), 100 ng/mL stem cell factor (SCF; catalog no. 255-SC; R&D Systems), 100 ng/mL FMS-like tyrosine kinase 3 ligand (FLT3L ; catalog no. 288-TP; R&D Systems), 50 ng/mL thrombopoietin (TPO) (catalog no. 308-FK; R&D Systems), and 100 nM UM171 (catalog no. 72912; Stemcell Technologies).

Chip control and setup

Microfluidic chips (C4F4-2020) were produced as described previously.[42] Microfluidic control manifolds, based on the solenoid valve controlled system at https://sites.google.com/site/rafaelsmicrofluidicspage/home, were used.[49] Flow layer liquids were pressurized to 0.25 bar, while 1.7 bar was sufficient to close all valves. Experimental scripting and control were conducted using a custom graphic user interface created using MATLAB (MathWorks).

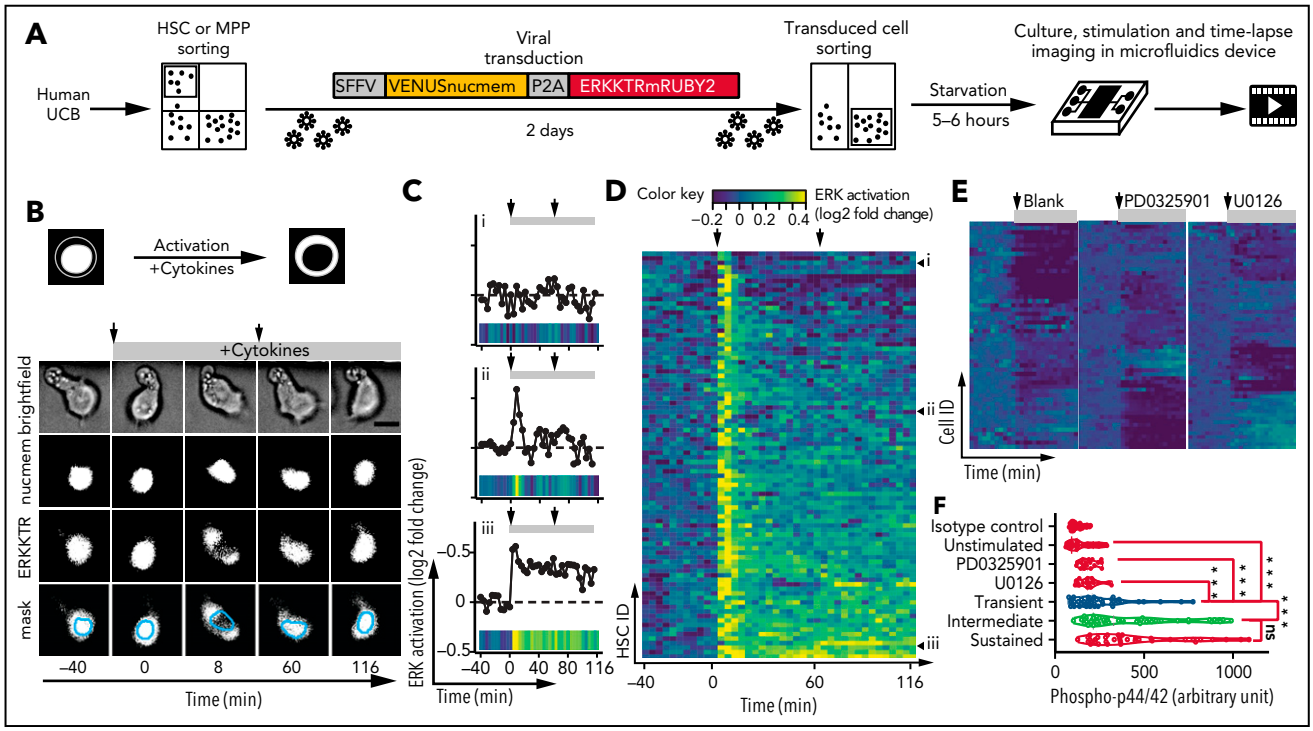

Figure 1. Live single-cell quantifications reveal heterogeneity in ERK signaling dynamics upon cytokine stimulation in human HSPCs. (A) Experimental scheme. The KTR-based fluorescent reporter is depicted to scale. (B) Schematic representation of the subcellular distribution of KTRs. When ERK is active, KTRs translocate from the nucleus to the cytoplasm, illustrated by representative video frames of a human HSC stimulated with 3F at indicated time. Shown are all 3 imaging channels and the overlay with the nuclear mask (scale bar, 10 μm). Gray bar at the top represents the timing of cytokine presence, and arrows indicate the timing of stimulation (media exchange) at 0 minutes and refreshment at 60 minutes. The same cell is shown in panel Cii and supplemental Video 2. (C) Single-cell time series and heat-stripe representation of ERK signaling response for 3 representative HSCs upon the stimulation with 3F. (D) Heat-stripe representation of ERK signaling dynamics in 90 single HSCs (3 independent experiments) in response to 3F. Each row corresponds to a single HSC, and cells are sorted based on cumulative ERK signal (no to high). Cells shown in panel C are highlighted in panels Di-iii). Two or 3 pooled UCB units were used per experiment. (E-F) Specificity of ERKKTR sensor. (E) Heat-stripe representation showing absence of ERK signaling in $CD34^+$ cells treated with blank medium (no 3F, 33 cells) and 3F plus ERK inhibitors PD0325901 (10 μM, 40 cells) or U0126 (10 μM, 44 cells) from 2 independent experiments. (F) Quantification of anti-phospho-p44/42 immunostaining 1 hour after stimulation of cells in panels D and E. Unpaired Student *t* test with Welch's correction. ***$P < .0005$; ns (not significant), $P > .05$. P2A , picornavirus 2A. SFFV, spleen focus-forming virus.

Time-lapse imaging

All time-lapse experiments were conducted at 37°C with a custom-made stage-top housing apparatus[42] that maintained 98% humidity, 5% O_2, and 5% CO_2. $VENUS^+mRUBY2^+$ cells were sorted, starved in the serum-free medium described above without cytokines for 5 to 6 hours. Brightfield and fluorescent images were acquired using a Nikon-Ti Eclipse microscopes, Hamamatsu Orca Flash 4.0 cameras, and 20× CFI Plan Apochromatic λ objectives (numerical aperture 0.45).

Short-term time-lapse experiments (156 minutes; Figures 1, 2, 3, and 4A-D) were conducted in microfluidic chips as described above. Cells were sorted, starved in cytokine-free medium containing anti-CD33 (APC, WM53, 6 ng/mL; BioLegend) or anti-CD71 (APC, CY1G4, 5 ng/mL; BioLegend) antibodies before loading onto the microfluidic chip. A fluorescent Alexa Fluor 700 (catalog no. A20010; ThermoFisher) dye was included in media containing cytokines to visualize media diffusion. Images were acquired every 4 minutes for a total of 156 minutes.

Long-term time-lapse experiments (3 days; Figure 4E-I) were conducted in channel slides (catalog no. 80606; ibidi). $VENUS^+mRUBY2^+$ cells were sorted and starved in cytokine-free medium containing anti-CD33 (APC, WM53, 6 ng/mL; BioLegend), anti-CD34 (BV421, 561, 20 ng/mL; BioLegend), and anti-CD45RA (BV480, HI100; BD Biosciences) antibodies before being seeded into ibidi channel slides coated with anti-human CD43 antibody (catalog no. 1B-220-C100; EXBIO).[50] Images were first acquired every 6 minutes for 120 minutes, followed by imaging of only CD45RA-BV480, CD34-BV421, and CD33-APC every 12 hours.

Generation and analysis of single-cell trajectories

Cell tracking and image quantification of fluorescent channels were performed as previously described.[26,28,51,52] For each cell and time point, the sum of nuclear fluorescence intensity of ERKKTRmRUBY2 was divided by the sum of (constantly expressed) VENUSnucmem fluorescence to correct for technical fluctuations in fluorescence intensity. Fold changes were then calculated by normalizing to the mean of baseline values (−40 to −4 minutes before cytokine stimulation). The resulting time series (decreased y-values for ERK activation) were mirrored along the horizontal axis to intuitively show ERK activity as an increase in y-value, and a value of 2 was added to all time points in order to reset the mean of baseline to 1 for each time series. Log2-transformed values were used for all subsequent analyses.

To classify "nonresponders" and "responders", the mean and standard deviation (SD) were calculated for the baseline (from

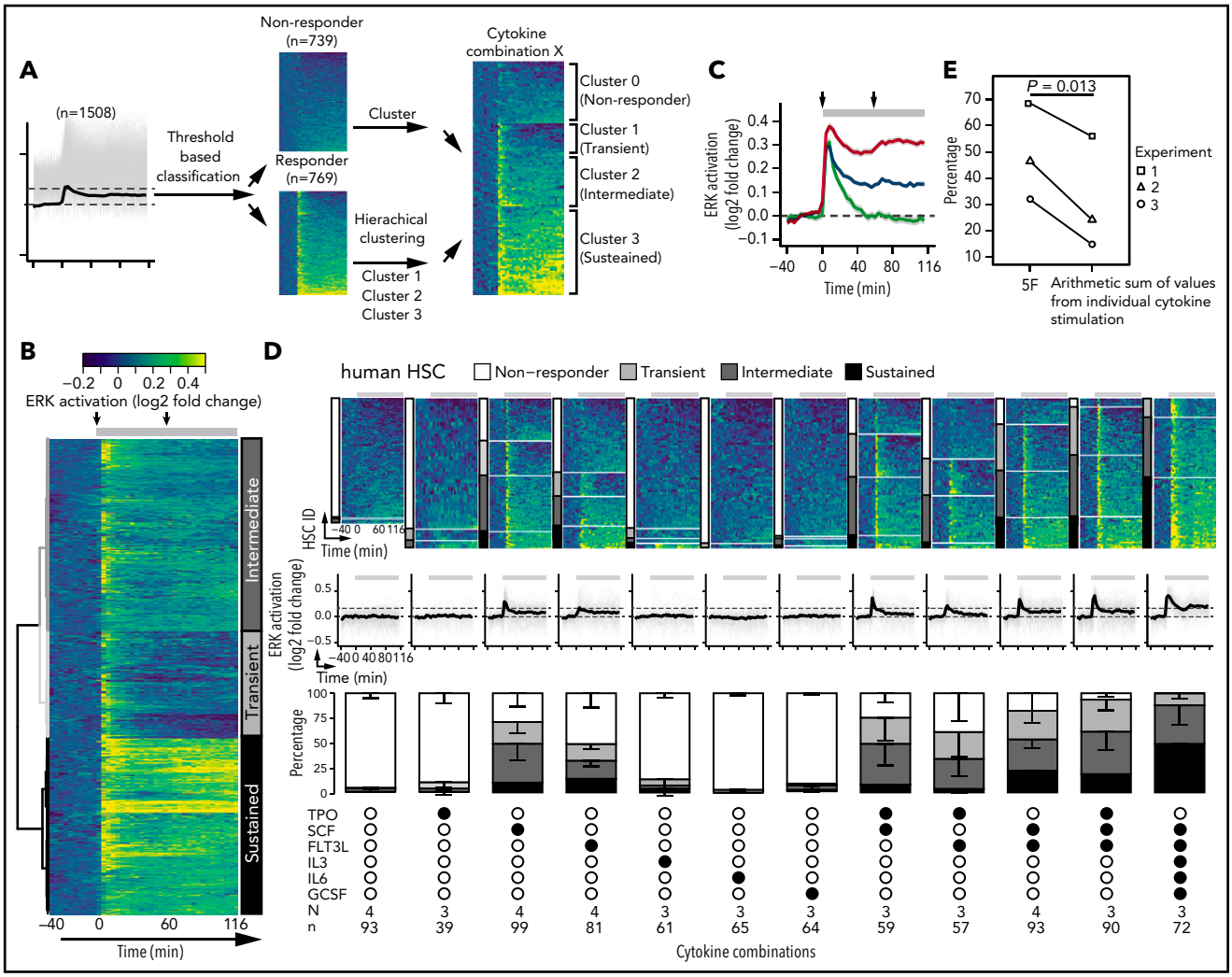

Figure 2. ERK signaling dynamics in human HSCs are dependent on cytokine identity and combinations. (A) Workflow of classifying clusters of different ERK signaling dynamics from pooled (n = 1508) single-cell time series of both HSCs and MPPs. (B) Hierarchical clustering of time series of responders (n = 769) using dynamic time warping and Ward's linkage method, resulting in 3 major clusters (transient, intermediate, and sustained) that are color coded. Gray bar at the top indicates the timing of cytokine presence, with arrows denoting the timing of stimulation and refreshment. (C) Population average of ERK signaling dynamics across 3 clusters as identified in panel B. Gray band indicates the 95% confidence interval of mean. (D) ERK signaling dynamics in single HSCs upon the stimulation with 12 different cytokine combinations are shown as heatmap (top panel) and time series (middle panel). For heatmaps, cells are organized according to the identified 4 clusters (nonresponder, transient, intermediate, and sustained) and sorted based on cumulative ERK signal (no to high). Heatmap heights are stretched to compensate for different cell numbers analyzed and best illustrate the frequencies of 4 clusters (scaled to 100%). For time series, gray curves represent individual cells, and black curve represents the population average. The 2 dashed lines denote values of 0 (bottom) and mean + 2xSD of the baseline measurements (top). Gray bar at the top indicates the timing of cytokine presence. Distributions of 4 clusters across 12 cytokine combinations (bottom panel) are calculated within individual experiments and shown as mean ± SD from 3 or 4 independent experiments (see supplemental Figure 5B for *P* values determined by pairwise Student *t* test with FDR correction). Black solid circles indicate the presence of cytokines. Number of independent experiments (N) performed and single cells (n) analyzed are shown. Two or 3 pooled UCB units were used per experiment. (E) 5F has a "more-than-additive" effect in inducing sustained ERK signaling dynamics. Shown are percentage of cells exhibiting sustained ERK activity upon the stimulation with 5F and the arithmetic sum of the corresponding 5 individual cytokine stimulations from 3 independent experiments (1-tailed, paired Student *t* test).

−40 to −4 minutes) values of all 1508 time series. For each cell, the average of 4 consecutive time points of the highest values was calculated in the time window of 0 to 40 minutes after cytokine stimulation, within which the initial response peak occurred. A cell was then defined as a responder if its average value was greater than the mean + 2xSD of the baseline measurements.

Hierarchical clustering of trajectories of responders was performed using a R/Shiny-based tool (Time Course Inspector).[53] Dynamic time warping as a distance measure and Ward's linkage method were used to construct the dendrogram.

ERK inhibitors and immunofluorescence staining

Cells were time-lapse imaged with or without 3F (100 ng/mL SCF, 50 ng/mL TPO, and 100 ng/mL FLT3L) stimulation and with or without 2 commonly used ERK pathway inhibitors (20 μM U0126 and 20 μM PD0325901), fixed 1 hour after stimulation with 4% paraformaldehyde (Sigma) for 20 minutes at room temperature, permeabilized with 0.2% Triton-X (Applichem), blocked for 1 hour in 10% donkey serum in TBS-T (Tris-buffered saline, 0.1% Tween 20), and stained with rabbit anti-phospho-p44/42 (9101; Cell Signaling Technology) primary antibodies in 10% donkey serum in TBS-T overnight at 4°C. Three washing steps (each lasting 5 minutes) was performed. Cells were then incubated with 10

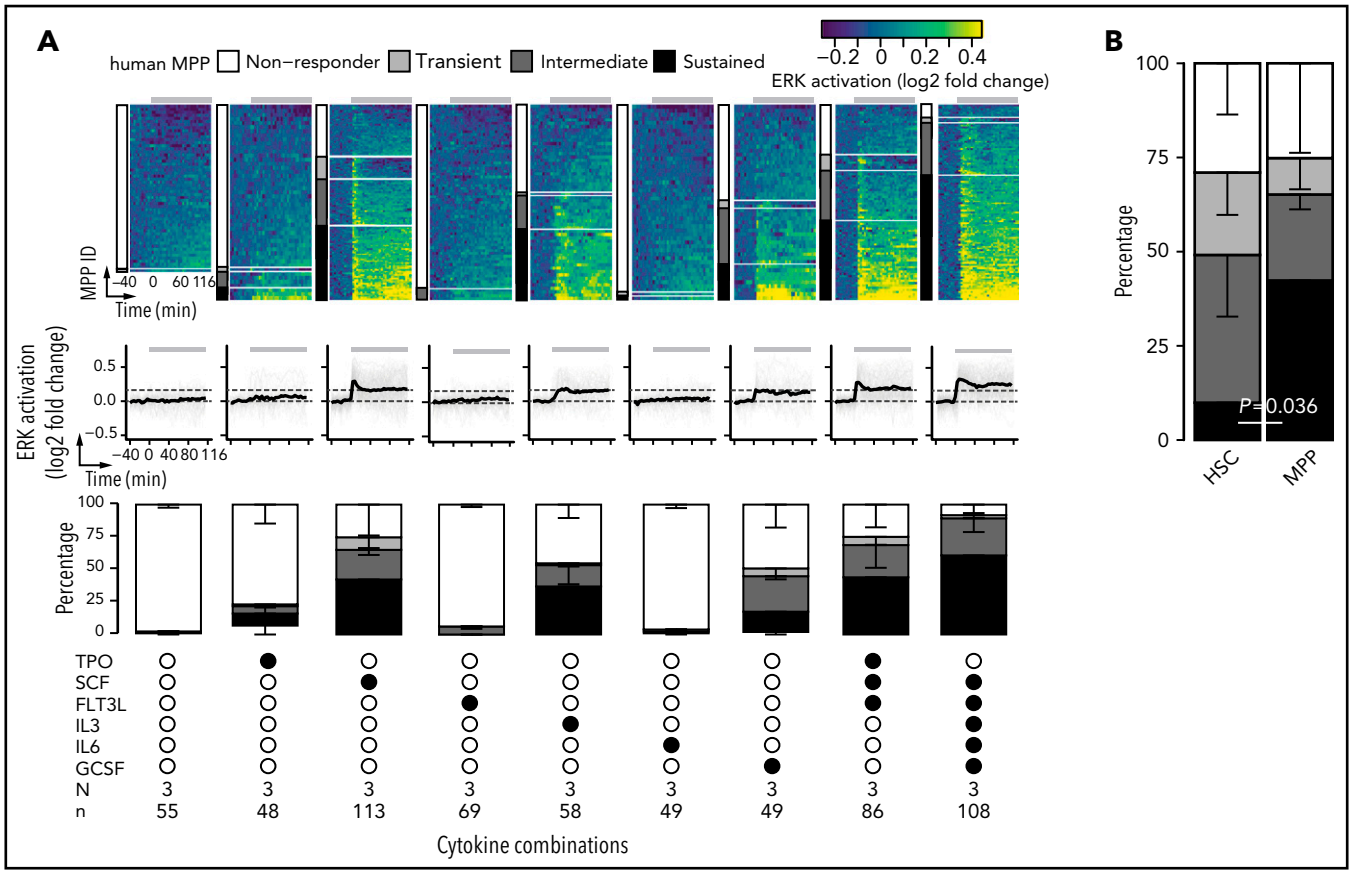

Figure 3. Cytokine-specific ERK signaling dynamics in human MPPs are cell-context dependent. (A) ERK signaling dynamics in single MPPs upon stimulation with 8 cytokine combinations are shown as heatmap (top panel) and time series (middle panel). For heatmaps, cells are organized according to the identified 4 clusters (non-responder, transient, intermediate, and sustained) and sorted based on cumulative ERK signal (low to high). Heatmap heights stretched to compensate for different cell numbers analyzed and best illustrate the distribution of 4 clusters (scaled to 100%). For time series, gray curves represent individual cells, and black curve represents the population average. The 2 dashed lines denote values of 0 (bottom) and mean + 2xSD of the baseline measurements (top). Gray bar at the top indicates the timing of cytokine presence. Distributions of 4 clusters across 8 cytokine combinations (bottom panel) are calculated within individual experiments and shown as mean ± SD from 3 independent experiments (see supplemental Figure 6B for *P* values determined by pairwise Student *t* test with FDR correction). Black solid circles indicate the presence of cytokines. Number of independent experiments (N) performed and single cells (n) analyzed are shown. Two or 3 pooled UCB units were used per experiment. (B) Percentage of HSCs vs MPPs displaying different ERK signaling dynamics upon SCF stimulation (2-tailed Student *t* test).

μg/mL Alexa Fluor 555 dye–conjugated donkey secondary antibodies (Invitrogen) for 3 hours at room temperature in 10% donkey serum in TBS-T, stained with 1 μg/mL 4′,6-diamidino-2-phenylindole for 10 min at room temperature, and imaged on a Nikon Eclipse Ti-E microscope using a CFI Plan Apo λ 20× objective (numerical aperture 0.75) and analyzed as described above.

Statistical analyses

Unpaired, 2-tailed Mann-Whitney *U* and Student *t* tests were performed to test the statistical significance of the data (unless otherwise stated); data normality was validated by the Shapiro-Wilk normality test in the latter case. False discovery rate (FDR) correction was applied for multiple comparisons. R (version 3.6.2) was used for all statistical analyses, with the α value set at 0.05.

Results

Live single-cell quantification reveals heterogeneity in ERK signaling dynamics upon human HSPC cytokine stimulation

We expressed VENUSnucmem[48] and ERKKTRmRUBY2[46] fusion proteins from a single lentiviral construct[7] in phenotypically enriched human UCB $CD34^+CD38^-CD45RA^-CD90^+CD49f^+$ "HSCs" (~10% functional HSCs capable of >6 months long-term repopulation in immunodeficient mice[45,54]) or $CD34^+CD38^-CD45RA^-CD90^-CD49f^-$ "MPPs"[54] (supplemental Figure 1). Lentiviral infection (Figure 1A) yielded 46% ± 10% (mean ± SD) and 37% ± 15% $VENUS^+mRUBY2^+$ cells, respectively, after 60 to 64 hours of culture (supplemental Figure 2). Transgene expressing cells were then sorted and starved for 5 to 6 hours before loading onto the microfluidics device (Figure 1A; supplemental Video 1). Cells were imaged every 4 minutes, starting at 40 minutes before stimulation to establish a baseline until 116 minutes after the first stimulation. Media containing different cytokines were delivered at 0 minutes and refreshed at 60 minutes. Media exchange by diffusion is rapid in the used microfluidic chip, and no relevant spatial or temporal gradients are created in the culture chambers.[42] Time-lapse images were analyzed by supervised tracking of single cells, segmentation of nuclei based on nuclear membrane fluorescent labeling by VENUSnucmem, and quantification of fluorescent intensity of both VENUSnucmem and nuclear ERKKTRmRUBY2 over time.[51,52] When ERK is phosphorylated (ie, activated), ERKKTRmRUBY2 translocates from the nucleus

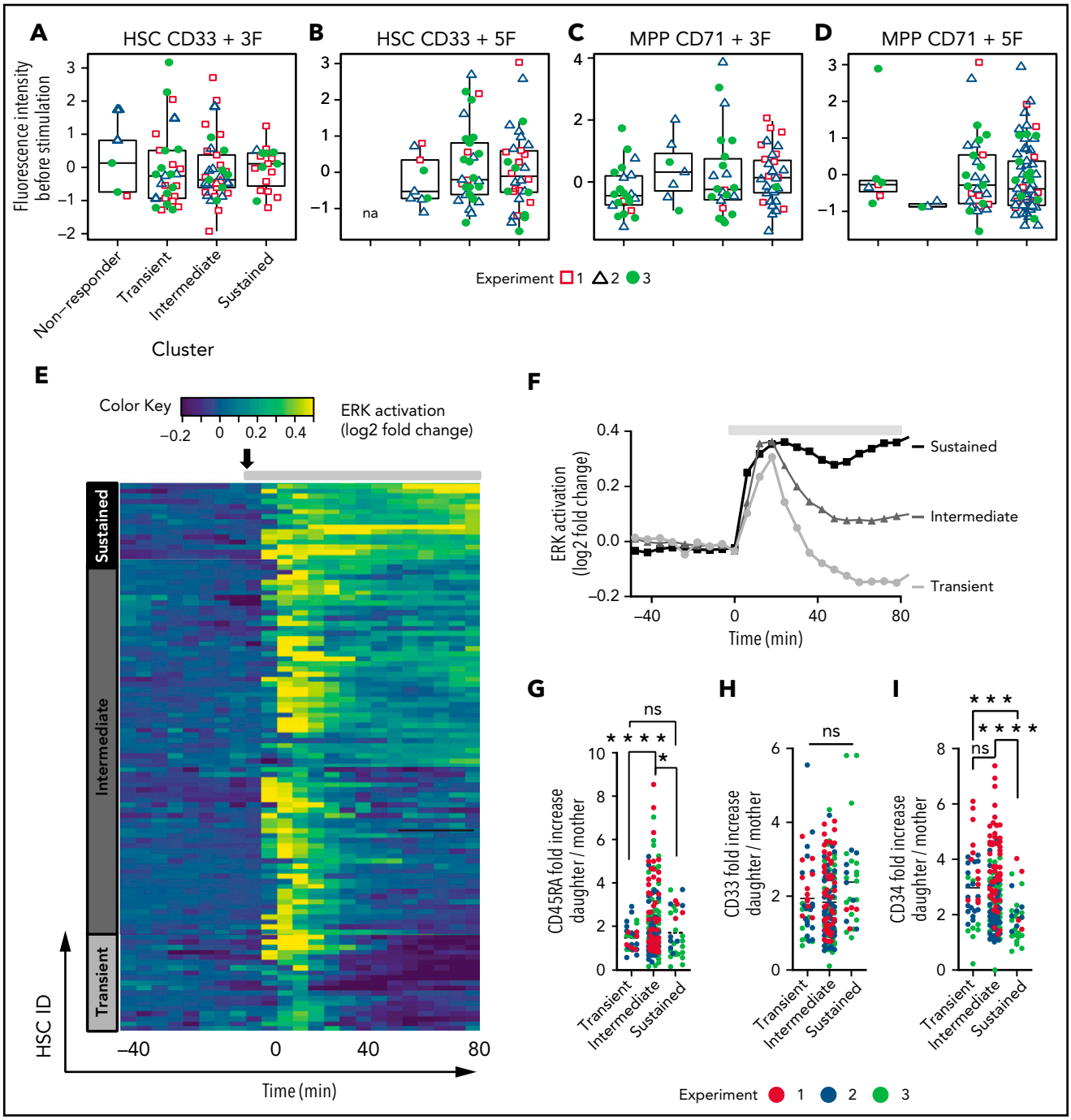

Figure 4. Known HSPC surface markers do not predict ERK signaling dynamics, but signaling dynamics predict future HSPC fates. (A-D) Expression levels of CD33 in HSCs and CD71 in MPPs were quantified for 10 time points before cytokine stimulation (−40 to −4 minutes). Average values for each cell were z-normalized within individual experiments. Pooled data from 3 independent experiments are shown, with symbols representing single cells. CD33 expression levels of HSCs exhibiting different ERK signaling dynamics are shown upon the stimulation of 3F (n = 90 cells) (A) and 5F (n = 72) (B). CD71 expression levels of MPPs are shown in response to 3F (n = 86) (C) and 5F (n = 108) (D). No statistical significance ($P > .05$) was detected between 4 clusters by pairwise Wilcoxon rank sum test with FDR correction. (E) ERK signaling dynamics in single HSCs upon 5F stimulation. Cells are organized according to the identified 3 clusters (transient, intermediate, and sustained) based on hierarchical clustering (dynamic time warping and Ward's linkage method) of responding cells (n = 109). Gray bar at the top indicates the timing of cytokine presence. Black solid arrow indicates the addition of cytokines. (F) Population average of ERK signaling dynamics in the 3 clusters identified in E. (G-I) ERK response dynamics predict CD45RA and CD34 expression in HSC daughter cells. Expression of CD45RA, CD33, and CD34 (average over a cell's lifetime) in HSCs and their progeny was quantified for 3 days after 5F stimulation. Statistical analysis by unpaired Student *t* test with Welch's correction. ****$P < .0001$; ***$P < .0005$; **$P < .005$; *$P < .05$; ns, $P > .05$.

to the cytoplasm (Figure 1B), thus enabling quantification of ERK activation dynamics in single cells (supplemental Video 2). We confirmed ERKKTR sensor specificity in human UCB CD34$^+$ cells by ERK inhibition with PD0325901 or U0126 and time-lapse imaging with subsequent end point immunostaining for phosphorylated ERK1/2 (phospho-p44/42) (Figure 1E-F). With the used experimental approach, HSPCs could be repeatedly stimulated (supplemental Figure 3).

We analyzed the effect of 6 cytokines, which are the components of cocktails reported to maintain or expand HSCs in culture. The first cocktail (3F)[43,44] contains 50 ng/mL TPO, 100 ng/mL SCF, and 100 ng/mL FLT3L. The second cocktail (5F)[45] contains 100 ng/mL SCF, 100 ng/mL FLT3L, 20 ng/mL interleukin 3 (IL-3), 20 ng/mL IL-6, and 20 ng/mL granulocyte colony-stimulating factor (GCSF). These cytokines have been previously reported to activate ERK in human and mouse HSPCs and cell lines,[16,55-59] but only by snapshot analysis, which is blind to single-cell dynamics. We stimulated human HSPCs with a total of 11 different conditions, including 6 individual cytokines and 5 different combinations. When HSCs were stimulated by 3F, it led to a peak of ERK activation within the first 12 minutes in almost all (94%) HSCs. However, the dynamics of ERK activation after the initial peak were heterogeneous between individual cells (Figure 1C-D). This demonstrates the feasibility of using ERKKTR to measure ERK signaling activation over time in HSCs and reveals high heterogeneity at the single-cell level.

Cytokine-induced ERK activation is cell-context dependent

To identify and quantify ERK signaling responses to different cytokines, we first pooled HSCs and MPPs from all cytokine combinations and used a threshold-based approach to classify cells as nonresponders and responders (Figure 2A). For each cell, the average of 4 consecutive highest values were obtained from 0 to 40 minutes after cytokine stimulation (initial response peak). A cell was defined as a responder if its mean was greater than the mean + 2xSD of the cell's baseline before stimulation.

Among the 6 individual cytokines, SCF and FLT3L were the main factors activating ERK in HSCs, with 71% ± 14% and 49% ± 14% of cells responding, respectively (supplemental Figure 4). The other cytokines elicited ERK responses only in a small number of HSCs (TPO: 10% ± 11%; IL-3: 13% ± 4%; IL-6: 3% ± 2%; GCSF: 8% ± 1%), which was not significantly different from the cytokine-free control condition (4% ± 5%; pairwise Student *t* test with FDR correction) (supplemental Figure 4). This is consistent with the ERK activation upon SCF or FLT3L stimulation detected by cytometry by time of flight in the same phenotypically defined HSC population,[16] confirming the specificity and sensitivity of our approach. Stimulation with combinations of cytokines increased the responder frequency. 3F and 5F stimulation led to 94% ± 4% and 100% ± 0% of HSCs responding, respectively (supplemental Figure 4), thus robustly activating most to all HSCs and reducing sample-to-sample variability (decreased SDs).

In contrast, SCF, IL-3, and GCSF were the main factors activating ERK in MPPs, with 75% ± 24%, 55% ± 10%, and 50% ± 18% of cells responding, respectively (supplemental Figure 4), significantly different from the cytokine-free control condition (1% ± 2%; pairwise Student *t* test with FDR correction). Fewer MPPs responded to 3F (75% ± 17%) and 5F (92% ± 7%) than HSCs ($P = .05$ and $P = 0.03$ respectively, 1-tailed Mann-Whitney *U* test) (supplemental Figure 4). Collectively, these data demonstrate the sensitivity of our approach and confirm the cellular context's influence on ERK signaling.

ERK signaling dynamics are cytokine and cell-type specific

To identify different types of ERK signaling dynamics, we applied hierarchical clustering with dynamic time warping[53] in responder cells (Figure 2A). Three major clusters emerged with distinct adaptive behavior (Figure 2B): 22% of cells displayed "transient" activation with full adaptation, where ERK activity returned to the basal level (mean + 2xSD of baseline measurements of all 1508 cells) by 60 minutes in 96% of these cells; 41% of cells exhibited "intermediate" adaptation, with 61% of these cells returning to basal ERK activity level by 60 minutes; and the remaining 37% of cells showed "sustained" activity for at least 88 minutes, with 89% of these cells staying above the basal level for the entire imaging period. Interestingly, the maximal level of ERK activation reached in the sustained cluster by 8 minutes of cytokine stimulation was significantly different from those of the transient and intermediate clusters ($P < .001$ by pairwise Mann-Whitney *U* test with FDR correction; Figure 2C).

To test if cytokines and their combinations lead to specific ERK signaling dynamics, we quantified the frequency of the 4 clusters (nonresponder, transient, intermediate, sustained) in response to cytokine stimulations in HSCs and MPPs. HSCs responded to SCF and FLT3L, but the 2 cytokines led to different frequencies of ERK activity dynamics (Figure 2D), specifically in intermediate responders (39% ± 16% and 18% ± 6%, respectively; $P = .049$ by pairwise Student *t* test with FDR correction; supplemental Figure 5). Distributions of the 3 different ERK signaling dynamics clusters upon the stimulation of 4 combinations among SCF, FLT3L, and TPO were similar to the sum of the effects by individual factors (supplemental Figure 5). Notably, 5F activated sustained ERK dynamics in 49% ± 18% of HSCs, which was significantly different from all the other tested cytokines alone or in combination. The arithmetic summation of the percentage of cells displaying sustained ERK activity when stimulated by the 5 corresponding cytokines individually was significantly lower than when activated by 5F (Figure 2E), illustrating a "more-than-additive" effect of the 5F together in eliciting sustained ERK signaling dynamics in HSCs.

In MPPs, SCF, IL-3, and GCSF stimulation resulted in a similar distribution of the 3 different ERK signaling dynamics clusters and an additive effect when combined (Figure 3A; supplemental Figure 6). Interestingly, fewer responding MPPs exhibited transient ERK dynamics than HSCs (8% vs 32%), while more showed sustained ERK activity (57% vs 23%) (supplemental Figure 7). Additionally, when HSCs and MPPs were activated by the same cytokine SCF, 14% ± 9% of responding HSCs vs 54% ± 17% of responding MPPs displayed sustained ERK dynamics ($P = .036$ by 2-tailed Student *t* test; Figure 3B). No significant difference was detected in the maximal ERK activity level between the 2 cell populations ($P = .71$ by 2-tailed Mann-Whitney *U* test).

For this study, we chose the cytokine concentrations previously shown to allow HSPC stimulations and maintenance.[43–45] Of note, not only cell type and cytokine identity but also their concentration impacts signaling activation. Decreasing SCF and FLT3L cytokine concentration increased the frequency of nonresponders while decreasing transient and intermediate responders (supplemental Figure 8).

Taken together, we demonstrate heterogeneous ERK signaling activity dynamics in HSCs and MPPs, which are dependent on both cell type and cytokine identity, their combinations and concentrations.

Current HSPC surface markers do not predict ERK signaling dynamics

Prospective isolation by currently available surface-marker combinations yields HSC and MPP subpopulations with distinct molecular and functional properties. The observed heterogeneity of ERK signaling dynamics could therefore reflect subpopulations with already-known differences in the expression of surface markers like CD33 (identifies a subset of HSCs with high regenerative potential[38]) and CD71 (a marker for metabolic activation[26] and a MPP subset with erythroid and megakaryocytic lineage potential[60]). We therefore quantified the expression levels of CD33 in HSCs and CD71 in MPPs prior to cytokine stimulation. We found no difference in CD33 or CD71 expression levels between the different ERK signaling dynamics clusters (Figure 4A-D,H). Thus, these 2 known surface markers do not identify HSPC subtypes with different ERK dynamics. ERK signaling dynamics could therefore enable the identification of novel currently unrecognized HSPC subtypes.

ERK signaling dynamics can identify HSPC subtypes with specific future behavior

Current protocols for prospective human HSCs enrichment yield a heterogeneous population.[54] To analyze whether ERK signaling response dynamics can identify cells with distinct future behavior, we stimulated HSCs with 5F, identified cells with 3 major ERK response dynamics by hierarchical clustering with dynamic time warping[53] (Figure 4E-F), and quantified future behavior and CD33, CD34, and CD45RA expression of these cells and their progeny by long-term single-cell imaging, tracking, and quantification.[6,26,28,61] Interestingly, HSCs with intermediate, but not with transient or sustained ERK dynamics upregulated CD45RA expression in the next (daughter) generation (Figure 4G). HSCs with transient and intermediate, but not with sustained, ERK dynamics retain higher CD34 expression in the next generation (Figure 4I). ERK signaling response dynamics thus enable identification of HSPC subtypes not distinguished by current surface markers.

Discussion

Cytokines control HSPC fates and are used for therapeutic ex vivo expansion[43,44,62-64] and genetic modification[65-67] of HSCs. SCF, FLT3L, TPO, IL-3, IL-6, and GCSF have been shown to directly control the survival, division, and regenerative potential of human HSPCs.[45,68] To dissect the mechanisms by which these cytokines mediate their effects, their downstream activation of multiple pathways were identified by cytometry by time of flight.[16] However, such analysis is limited to snapshots and thus blind to the dynamics of signaling activity at the single-cell level, which holds crucial information for controlling cell fates.[23] This is especially important for heterogeneous cell populations such as HSPCs. Here, we established the use of biosensors with time-lapse imaging and a dedicated automated microfluidics platform to enable continuous quantification of signaling activation dynamics over time in live, single human HSCs and MPPs. ERK dynamics were highly heterogeneous between individual cells, specific to cytokine identity and combinations, and significantly different between these 2 closely related cell types. This demonstrates the necessity to continuously measure signaling responses directly in the cell type of interest upon input signals with defined combinations and dose and temporal patterns. Additionally, the new technologies established here can be applied to different HSPCs and other rare suspension cell systems, and the single-cell data generated is a valuable resource for modeling approaches to identify molecular players that shape ERK signaling dynamics specific to cytokines[34,35] and cell types.[69]

Cell-to-cell variability in signaling is attributed to (1) the existence of different cell subtypes[38,60,70] or cell states[71,72] in the phenotypically defined HSC and MPP compartments and (2) the intrinsic variability within signaling networks.[73-75] We did not find a correlation between different ERK signaling dynamics and the expression level of CD33 and CD71, which are currently known markers to identify HSC and MPP subtypes,[38,60] respectively. Thus, it was possible that ERK signaling dynamics provide an additional noninvasive dimension of cellular properties to enable the identification of novel HSPC types that are currently indistinguishable by surface markers or morphology. Indeed, ERK signaling dynamics correlated with future cell behavior, thus identifying subtypes within the prospectively enriched HSC population; CD45RA expression increased more in daughters of HSCs with intermediate than with transient or sustained ERK signaling. Whether these different signaling response dynamics are a mere phenotype of different already-committed cell types or are also functionally responsible for instructing specific future fates will be interesting to analyze in the future. Signaling dynamics were shown to differ between cell types in other cell systems due to cell-type–specific network structures[36] and pathways crosstalk.[76] On the other hand, signaling heterogeneity can allows a homogenous population of cells to respond differently to uniform stimuli,[34,76] which is evolutionarily beneficial to confer population response robustness.[77–80] Therefore, capturing heterogeneity in signaling dynamics in individual HSPCs is crucial to understand its functional consequences at both the cellular and system levels.

Of the analyzed 6 individual cytokines, SCF and FLT3L activated ERK in HSCs, whereas SCF, IL-3, and GCSF elicited ERK responses in MPPs. Our results are consistent with previous snapshot analyses of HSCs.[16] However, ERK responses to the same cytokines were previously not detected in MPPs, further demonstrating the sensitivity of our approach. Furthermore, SCF induced sustained ERK dynamics in fewer HSCs than MPPs, despite similar response amplitudes. A higher baseline activity level in HSCs than in MPPs has previously been reported for multiple signaling molecules, including ERK.[16] These findings suggest that intracellular signaling pathways are wired and regulated differently in HSCs and MPPs, which is a crucial prerequisite for targeted manipulation of signaling to control cell fate.[79] Such cell-type–specific signaling dynamics could also be useful in situations where healthy and diseased cells differ in their signaling response.[82,83] Signaling dynamics can thus serve as a biomarker to distinguish cells that may be targeted by small molecules or other perturbations to achieve therapeutic specificity.

Combinatorial effects of cytokines affect signaling dynamics[17] and cellular function.[7,25,45] Notably, stimulation with cytokine combinations resulted in increased frequency of responding cells over the same cytokines individually. 5F, which allows HSC maintenance in culture for 21 days,[45] activated ERK in all HSCs. Strikingly, 5F also had a synergistic effect in activating sustained ERK dynamics over SCF and FLT3L, although IL-3, IL-6, and GCSF did not activate ERK on their own. This demonstrates crosstalk at either the receptor level or downstream pathways between SCF, FLT3L, and at least 1 of the remaining 3 cytokines. Elevated β-catenin levels have been shown to be exclusive upon 5F stimulation and increase cell survival and proliferation in human HSCs.[16] Given a direct link between ERK

and upregulation of β-catenin,[84] sustained ERK dynamics might be relevant for the activation of β-catenin in HSCs. In addition, an ERK-dependent feedback mechanism has been reported to prevent the exhaustion of mouse bone marrow HSCs and human $CD34^+CD38^-$ progenitor cells by returning them to the quiescent state once activated.[85] Taken together, these findings indicate that ERK signaling dynamics might play an important role in regulating human HSC function. Further investigation of the underlying molecular mechanisms that interpret and translate signaling dynamics into cellular responses will provide important insights into how the long-term regenerative capacity unique to HSCs is regulated and identify potential targets for pharmacological manipulation to increase HSC self-renewal divisions. The approaches we developed here pave the way for these analyses and combinatorial drug screening[86,87] to manipulate signaling dynamics for improved treatments of hematopoietic malignancies.

Acknowledgments

The authors thank the D-BSSE Single Cell and Clean Room Facilities for technical support.

This project was supported by Swiss National Science Foundation grant 179490 (T.S.), and a SystemsX Swiss Initiative in Systems Biology Transition postdoctoral fellowship and ETH Career Seed Grant SEED-16 17-2 (W.W.).

Authorship

Contribution: W.W. and Y.Z. designed and performed experiments, analyzed data, and wrote the paper with T.S.; P.D. designed and produced the microfluidics device; A.R. and T.K. assisted with biosensor development and data analysis; D.L. and T.K. maintained long-term bioimaging; M.G.M. and C.L. provided human UCB samples; T.S. designed and supervised the study; and all authors read and approved the final manuscript.

Conflict-of-interest disclosure: The authors declare no competing financial interests.

ORCID profiles: Y.Z., 0000-0002-1763-6908; T.K., 0000-0001-8002-0519; C.L., 0000-0001-5442-2805; T.S., 0000-0001-9320-0252.

Correspondence: Timm Schroeder, Department of Biosystems Science and Engineering, ETH Zurich, Mattenstrasse 26, 4058 Basel, Switzerland; e-mail: timm.schroeder@bsse.ethz.ch.

Footnotes

Submitted 3 August 2020; accepted 23 April 2021; prepublished online on Blood First Edition 14 May 2021. DOI 10.1182/blood.2020008386.

*W.W. and Y.Z. contributed equally to this study.

Source data are available from the corresponding author upon request.

The online version of this article contains a data supplement.

The publication costs of this article were defrayed in part by page charge payment. Therefore, and solely to indicate this fact, this article is hereby marked "advertisement" in accordance with 18 USC section 1734.

REFERENCES

1. Pietras EM, Mirantes-Barbeito C, Fong S, et al. Chronic interleukin-1 exposure drives haematopoietic stem cells towards precocious myeloid differentiation at the expense of self-renewal. *Nat Cell Biol.* 2016;18(6):607-618.
2. Etzrodt M, Ahmed N, Hoppe PS, et al. Inflammatory signals directly instruct PU.1 in HSCs via TNF. *Blood.* 2019;133(8):816-819.
3. Wang W, Fujii H, Kim HJ, et al. Enhanced human hematopoietic stem and progenitor cell engraftment by blocking donor T cell-mediated TNFα signaling. *Sci Transl Med.* 2017;9(421):eaag3214.
4. Baldridge MT, King KY, Boles NC, Weksberg DC, Goodell MA. Quiescent haematopoietic stem cells are activated by IFN-γ in response to chronic infection. *Nature.* 2010;465(7299):793-797.
5. Essers MAG, Offner S, Blanco-Bose WE, et al. IFNalpha activates dormant haematopoietic stem cells in vivo. *Nature.* 2009;458(7240):904-908.
6. Rieger MA, Hoppe PS, Smejkal BM, Eitelhuber AC, Schroeder T. Hematopoietic cytokines can instruct lineage choice. *Science* 2009;325(5937):217-218.
7. Endele M, Loeffler D, Kokkaliaris KD, et al. CSF-1-induced Src signaling can instruct monocytic lineage choice. *Blood.* 2017;129(12):1691-1701.
8. Yilmaz ÖH, Valdez R, Theisen BK, et al. Pten dependence distinguishes haematopoietic stem cells from leukaemia-initiating cells. *Nature.* 2006;441(7092):475-482.
9. Guzman ML, Neering SJ, Upchurch D, et al. Nuclear factor-κB is constitutively activated in primitive human acute myelogenous leukemia cells. *Blood.* 2001;98(8):2301-2307.
10. Kharas MG, Okabe R, Ganis JJ, et al. Constitutively active AKT depletes hematopoietic stem cells and induces leukemia in mice. *Blood.* 2010;115(7):1406-1415.
11. Chung E, Kondo M. Role of Ras/Raf/MEK/ERK signaling in physiological hematopoiesis and leukemia development. *Immunol Res.* 2011;49(1-3):248-268.
12. Wilkinson AC, Igarashi KJ, Nakauchi H. Haematopoietic stem cell self-renewal in vivo and ex vivo. *Nat Rev Genet.* 2020;21(9):541-554.
13. Coutu DL, Kokkaliaris KD, Kunz L, Schroeder T. Three-dimensional map of nonhematopoietic bone and bone-marrow cells and molecules. *Nat Biotechnol.* 2017;35(12):1202-1210.
14. Kunz L, Schroeder T. A 3D tissue-wide digital imaging pipeline for quantitation of secreted molecules shows absence of CXCL12 gradients in bone marrow. *Cell Stem Cell.* 2019;25(6):846-854.e4.
15. Coutu DL, Kokkaliaris KD, Kunz L, Schroeder T. Multicolor quantitative confocal imaging cytometry. *Nat Methods.* 2018;15(1):39-46.
16. Knapp DJHF, Hammond CA, Aghaeepour N, et al. Distinct signaling programs control human hematopoietic stem cell survival and proliferation. *Blood.* 2017;129(3):307-318.
17. Wang W, Akbarian V, Audet J. Biochemical measurements on single erythroid progenitor cells shed light on the combinatorial regulation of red blood cell production. *Mol Biosyst.* 2013;9(2):234-245.
18. Endele M, Etzrodt M, Schroeder T. Instruction of hematopoietic lineage choice by cytokine signaling. *Exp Cell Res.* 2014;329(2):207-213.
19. Barberis M, Helikar T, Verbruggen P. Simulation of stimulation: cytokine dosage and cell cycle crosstalk driving timing-dependent T cell differentiation. *Front Physiol.* 2018;9:879.
20. Rieger MA, Schroeder T. Analyzing cell fate control by cytokines through continuous single cell biochemistry. *J Cell Biochem.* 2009;108(2):343-352.
21. Kellogg RA, Tay S. Noise facilitates transcriptional control under dynamic inputs. *Cell.* 2015;160(3):381-392.
22. Ryu H, Chung M, Dobrzyński M, et al. Frequency modulation of ERK activation dynamics rewires cell fate. *Mol Syst Biol.* 2015;11(11):838.

23. Purvis JE, Lahav G. Encoding and decoding cellular information through signaling dynamics. *Cell*. 2013;152(5):945-956.

24. Marshall CJ. Specificity of receptor tyrosine kinase signaling: transient versus sustained extracellular signal-regulated kinase activation. *Cell*. 1995;80(2):179-185.

25. Endele M, Schroeder T. Molecular live cell bioimaging in stem cell research. *Ann N Y Acad Sci*. 2012;1266(1):18-27.

26. Loeffler D, Wehling A, Schneiter F, et al. Asymmetric lysosome inheritance predicts activation of haematopoietic stem cells [published correction appears in *Nature*. 573;E5]. *Nature*. 2019;573(7774):426-429.

27. Loeffler D, Schroeder T. Understanding cell fate control by continuous single-cell quantification. *Blood*. 2019;133(13):1406-1414.

28. Hoppe PS, Schwarzfischer M, Loeffler D, et al. Early myeloid lineage choice is not initiated by random PU.1 to GATA1 protein ratios. *Nature*. 2016;535(7611):299-302.

29. Regot S, Hughey JJ, Bajar BT, Carrasco S, Covert MW. High-sensitivity measurements of multiple kinase activities in live single cells. *Cell*. 2014;157(7):1724-1734.

30. Kudo T, Jeknić S, Macklin DN, et al. Live-cell measurements of kinase activity in single cells using translocation reporters. *Nat Protoc*. 2018;13(1):155-169.

31. Lahav G, Rosenfeld N, Sigal A, et al. Dynamics of the p53-Mdm2 feedback loop in individual cells. *Nat Genet*. 2004;36(2):147-150.

32. Tay S, Hughey JJ, Lee TK, Lipniacki T, Quake SR, Covert MW. Single-cell NF-kappaB dynamics reveal digital activation and analogue information processing. *Nature*. 2010; 466(7303):267-271.

33. Tyas L, Brophy VA, Pope A, Rivett AJ, Tavaré JM. Rapid caspase-3 activation during apoptosis revealed using fluorescence-resonance energy transfer. *EMBO Rep*. 2000;1(3):266-270.

34. Blum Y, Mikelson J, Dobrzyński M, et al. Temporal perturbation of ERK dynamics reveals network architecture of FGF2/MAPK signaling. *Mol Syst Biol*. 2019;15(11):e8947.

35. Santos SDM, Verveer PJ, Bastiaens PIH. Growth factor-induced MAPK network topology shapes Erk response determining PC-12 cell fate. *Nat Cell Biol*. 2007;9(3):324-330.

36. Martin EW, Pacholewska A, Patel H, Dashora H, Sung MH. Integrative analysis suggests cell type-specific decoding of NF-κB dynamics. *Sci Signal*. 2020;13(620):eaax7195.

37. Cheung AMS, Nguyen LV, Carles A, et al. Analysis of the clonal growth and differentiation dynamics of primitive barcoded human cord blood cells in NSG mice. *Blood*. 2013;122(18):3129-3137.

38. Knapp DJHF, Hammond CA, Hui T, et al. Single-cell analysis identifies a $CD33^{+}$ subset of human cord blood cells with high regenerative potential. *Nat Cell Biol*. 2018;20(6):710-720.

39. Schroeder T. Tracking hematopoiesis at the single cell level. *Ann N Y Acad Sci*. 2005;1044(1):201-209.

40. Etzrodt M, Endele M, Schroeder T. Quantitative single-cell approaches to stem cell research. *Cell Stem Cell*. 2014;15(5):546-558.

41. Hoppe PS, Coutu DL, Schroeder T. Single-cell technologies sharpen up mammalian stem cell research. *Nat Cell Biol*. 2014;16(10):919-927.

42. Dettinger P, Wang W, Ahmed N, et al. An automated microfluidic system for efficient capture of rare cells and rapid flow-free stimulation. *Lab Chip*. 2020;20(22):4246-4254.

43. Csaszar E, Kirouac DC, Yu M, et al. Rapid expansion of human hematopoietic stem cells by automated control of inhibitory feedback signaling. *Cell Stem Cell*. 2012;10(2):218-229.

44. Fares I, Chagraoui J, Gareau Y, et al. Pyrimidoindole derivatives are agonists of human hematopoietic stem cell self-renewal. *Science* 2014;345(6203):1509-1512.

45. Knapp DJHF, Hammond CA, Miller PH, et al. Dissociation of survival, proliferation, and state control in human hematopoietic stem cells. *Stem Cell Reports*. 2017;8(1):152-162.

46. Lam AJ, St-Pierre F, Gong Y, et al. Improving FRET dynamic range with bright green and red fluorescent proteins. *Nat Methods*. 2012; 9(10):1005-1012.

47. Koushik SV, Chen H, Thaler C, Puhl HL III, Vogel SS. Cerulean, venus, and venusY67C FRET reference standards. *Biophys J*. 2006; 91(12):L99-L101.

48. Okita C, Sato M, Schroeder T. Generation of optimized yellow and red fluorescent proteins with distinct subcellular localization. *Biotechniques*. 2004;36(3):418-422, 424.

49. Kellogg RA, Gómez-Sjöberg R, Leyrat AA, Tay S. High-throughput microfluidic single-cell analysis pipeline for studies of signaling dynamics. *Nat Protoc*. 2014;9(7):1713-1726.

50. Loeffler D, Wang W, Hopf A, et al. Mouse and human HSPC immobilization in liquid culture by CD43- or CD44-antibody coating. *Blood*. 2018;131(13):1425-1429.

51. Hilsenbeck O, Schwarzfischer M, Skylaki S, et al. Software tools for single-cell tracking and quantification of cellular and molecular properties. *Nat Biotechnol*. 2016;34(7):703-706.

52. Hilsenbeck O, Schwarzfischer M, Loeffler D, et al. fastER: a user-friendly tool for ultrafast and robust cell segmentation in large-scale microscopy. *Bioinformatics*. 2017;33(13): 2020-2028.

53. Dobrzyński M, Jacques M-A, Pertz O. Mining single-cell time-series datasets with Time Course Inspector. *Bioinformatics*. 2020;36(6): 1968-1969.

54. Notta F, Doulatov S, Laurenti E, et al. Isolation of single human hematopoietic stem cells capable of long-term multilineage engraftment. *Science* 2011;333(6039):218-221.

55. Nonami A, Kato R, Taniguchi K, et al. Spred-1 negatively regulates interleukin-3-mediated ERK/mitogen-activated protein (MAP) kinase activation in hematopoietic cells. *J Biol Chem*. 2004;279(50):52543-52551.

56. Kamata T, Pritchard CA, Leavitt AD. Raf-1 is not required for megakaryocytopoiesis or TPO-induced ERK phosphorylation. *Blood*. 2004;103(7):2568-2570.

57. Kent D, Copley M, Benz C, Dykstra B, Bowie M, Eaves C. Regulation of hematopoietic stem cells by the steel factor/KIT signaling pathway. *Clin Cancer Res*. 2008;14(7):1926-1930.

58. Maeda K, Malykhin A, Teague-Weber BN, Sun XH, Farris AD, Coggeshall KM. Interleukin-6 aborts lymphopoiesis and elevates production of myeloid cells in systemic lupus erythematosus-prone B6.Sle1.Yaa animals. *Blood*. 2009;113(19): 4534-4540.

59. Kamezaki K, Shimoda K, Numata A, et al. Roles of Stat3 and ERK in G-CSF signaling. *Stem Cells*. 2005;23(2):252-263.

60. Notta F, Zandi S, Takayama N, et al. Distinct routes of lineage development reshape the human blood hierarchy across ontogeny. *Science* 2016;351(6269):aab2116.

61. Eilken HM, Nishikawa S, Schroeder T. Continuous single-cell imaging of blood generation from haemogenic endothelium. *Nature*. 2009;457(7231):896-900.

62. Boitano AE, Wang J, Romeo R, et al. Aryl hydrocarbon receptor antagonists promote the expansion of human hematopoietic stem cells. *Science* 2010;329(5997):1345-1348.

63. Wagner JE Jr, Brunstein CG, Boitano AE, et al. Phase I/II trial of StemRegenin-1 expanded umbilical cord blood hematopoietic stem cells supports testing as a stand-alone graft. *Cell Stem Cell*. 2016;18(1):144-155.

64. Cohen S, Roy J, Lachance S, et al. Hematopoietic stem cell transplantation using single UM171-expanded cord blood: a single-arm, phase 1-2 safety and feasibility study. *Lancet Haematol*. 2020;7(2):e134-e145.

65. Naldini L. Gene therapy returns to centre stage. *Nature*. 2015;526(7573):351-360.

66. Aiuti A, Biasco L, Scaramuzza S, et al. Lentiviral hematopoietic stem cell gene therapy in patients with wiskott-aldrich syndrome. *Science* 2013;341(6148):1233151.

67. Genovese P, Schiroli G, Escobar G, et al. Targeted genome editing in human repopulating haematopoietic stem cells. *Nature*. 2014;510(7504):235-240.

68. Petzer AL, Zandstra PW, Piret JM, Eaves CJ. Differential cytokine effects on primitive (CD34+CD38-) human hematopoietic cells: novel responses to Flt3-ligand and thrombopoietin. *J Exp Med*. 1996;183(6):2551-2558.

69. Brandt R, Sell T, Lüthen M, et al. Cell type-dependent differential activation of ERK by oncogenic KRAS in colon cancer and intestinal epithelium. *Nat Commun*. 2019;10(1): 2919.

70. Schroeder T. Hematopoietic stem cell heterogeneity: subtypes, not unpredictable behavior. *Cell Stem Cell*. 2010;6(3):203-207.

71. Yu VWC, Yusuf RZ, Oki T, et al. Epigenetic memory underlies cell-autonomous heterogeneous behavior of hematopoietic stem cells [published correction appears in *Cell*. 2017;168(5):944–945]. *Cell*. 2016;167(5):1310-1322.e17.

72. Farlik M, Halbritter F, Müller F, et al. DNA methylation dynamics of human hematopoietic stem cell differentiation. *Cell Stem Cell*. 2016;19(6):808-822.

73. Bhalla US. Signaling in small subcellular volumes. I. Stochastic and diffusion effects on individual pathways. *Biophys J*. 2004;87(2):733-744.

74. Fritsche-Guenther R, Witzel F, Sieber A, et al. Strong negative feedback from Erk to Raf confers robustness to MAPK signalling. *Mol Syst Biol*. 2011;7(1):489.

75. Sigal A, Milo R, Cohen A, et al. Variability and memory of protein levels in human cells. *Nature*. 2006;444(7119):643-646.

76. Chen JY, Lin JR, Cimprich KA, Meyer T. A two-dimensional ERK-AKT signaling code for an NGF-triggered cell-fate decision. *Mol Cell*. 2012;45(2):196-209.

77. Wollman R. Robustness, accuracy, and cell state heterogeneity in biological systems. *Curr Opin Syst Biol*. 2018;8:46-50.

78. Selimkhanov J, Taylor B, Yao J, et al. Accurate information transmission through dynamic biochemical signaling networks. *Science* 2014;346(6215):1370-1373.

79. Paszek P, Ryan S, Ashall L, et al. Population robustness arising from cellular heterogeneity. *Proc Natl Acad Sci U S A*. 2010;107(25):11644-11649.

80. Suderman R, Bachman JA, Smith A, Sorger PK, Deeds EJ. Fundamental trade-offs between information flow in single cells and cellular populations. *Proc Natl Acad Sci U S A*. 2017;114(22):5755-5760.

81. Behar M, Barken D, Werner SL, Hoffmann A. The dynamics of signaling as a pharmacological target. *Cell*. 2013;155(2):448-461.

82. Francisco DC, Peddi P, Hair JM, et al. Induction and processing of complex DNA damage in human breast cancer cells MCF-7 and nonmalignant MCF-10A cells. *Free Radic Biol Med*. 2008;44(4):558-569.

83. Bugaj LJ, Sabnis AJ, Mitchell A, et al. Cancer mutations and targeted drugs can disrupt dynamic signal encoding by the Ras-Erk pathway. *Science* 2018;361(6405):eaao3048.

84. Ding Q, Xia W, Liu JC, et al. Erk associates with and primes GSK-3β for its inactivation resulting in upregulation of β-catenin. *Mol Cell*. 2005;19(2):159-170.

85. Baumgartner C, Toifl S, Farlik M, et al. An ERK-dependent feedback mechanism prevents hematopoietic stem cell exhaustion. *Cell Stem Cell*. 2018;22(6):879-892.e6.

86. Goglia AG, Wilson MZ, Jena SG, et al. A live-cell screen for altered Erk dynamics reveals principles of proliferative control. *Cell Syst*. 2020;10(3):240-253.e6.

87. Klinger B, Sieber A, Fritsche-Guenther R, et al. Network quantification of EGFR signaling unveils potential for targeted combination therapy. *Mol Syst Biol*. 2013;9(1):673.